Tuning the crystal structure of $A_2CoPO_4F(A = Li, Na)$ fluoride-phosphates : a new layered polymorph of $LiNaCoPO_4F$

EurJIC
European Journal of Inorganic Chemistry

A Journal of ChemPubSoc Europe

Accepted Article

Title: Tuning the crystal structure of A2CoPO4F (A = Li, Na) fluoride-phosphates: a new layered polymorph of LiNaCoPO4F

Authors: Stanislav Fedotov, Dmitry Aksyonov, Aleksandr Samarin, Olesia Karakulina, Joke Hadermann, Keith Stevenson, Nellie Khasanova, Artem Abakumov, and Evgeny Antipov

To be cited as: *Eur. J. Inorg. Chem.* 10.1002/ejic.201900660

Link to VoR: http://dx.doi.org/10.1002/ejic.201900660

WILEY-VCH

WILEY-VCH

FULL PAPER

Tuning the crystal structure of A_2CoPO_4F (A = Li, Na) fluoride-phosphates: a new layered polymorph of $LiNaCoPO_4F$

Stanislav S. Fedotov[a], *, Dmitry A. Aksyonov[a], Aleksandr Sh. Samarin[b], Olesia M. Karakulina[c], Joke Hadermann[c], Keith J. Stevenson[a], Nellie R. Khasanova[b], Artem M. Abakumov[a], Evgeny V. Antipov[b], [a], *

Abstract: Co-containing fluoride-phosphates are of interest in sense of delivering high electrode potentials and attractive specific energy values as positive electrode materials for rechargeable batteries. In this paper we report on a new Co-based fluoride-phosphate, $LiNaCoPO_4F$, with a layered structure (2D), which was Rietveld-refined based on X-ray powder diffraction data ($P2_1/c$, a = 6.83881(4) Å, b = 11.23323(5) Å, c = 5.07654(2) Å, β = 90.3517(5) °, V = 389.982(3) Å^3) and validated by electron diffraction and high-resolution scanning transmission electron microscopy. The differential scanning calorimetry measurements revealed that 2D-$LiNaCoPO_4F$ forms in a narrow temperature range of 520-530°C and irreversibly converts to the known 3D-$LiNaCoPO_4F$ modification (*Pnma*) above 530°C. The non-carbon-coated 2D-$LiNaCoPO_4F$ shows reversible electrochemical activity in Li-ion cell in the potential range of 3.0-4.9 V vs. Li/Li^+ with an average potential of ~4.5V and in Na-ion cell in the range of 3.0-4.5 V vs. Na/Na^+ exhibiting a plateau profile centred around 4.2 V, in agreement with the calculated potentials by density functional theory. The energy barriers for both Li^+ and Na^+ migration in 2D-$LiNaCoPO_4F$ amount to 0.15 eV along the [001] direction rendering 2D-$LiNaCoPO_4F$ as a viable electrode material for high-power Li- and Na-ion rechargeable batteries. The discovery and stabilization of the 2D-$LiNaCoPO_4F$ polymorph indicates that temperature influence on the synthesis of A_2MPO_4F fluoride-phosphates needs more careful examination with perspective to unveil new structures.

Introduction

A major breakthrough in the battery industry was hallmarked by the birth of Lithium-ion technology. Originally designed to unplug electronic devices, today these batteries eagerly power electric cars and buffer-store energy from renewable sources. Key performance indicators of the Li-ion battery (specific energy, power and operating life) are largely determined by the positive electrode (or cathode). Since Goodenough and co-workers proposed layered $LiCoO_2$ as a cathode[1], an immense number of candidates have been nominated for this role. The success of the now commercialized olivine-type $LiFePO_4$[2] boosted the investigation of XO_m^{n-} polyanion compounds, which offer better structural, thermal and cycling stability[3]. Recently, mixed anion materials like fluoride-phosphates have drawn a lot of attention owing to a possibility of synergizing the advantages of both anion moieties. For instance, a cooperative «inductive effect» of the anions brings the operating electrode potential to much higher values in comparison to oxides. Moreover, a better ionic transport is expected owing to a lower affinity of alkali metals towards fluoride than oxide anions. A much richer structural diversity of fluoride-phosphates offers manifold options for tuning the electrochemical properties [4].

Among fluoride-phosphates the A_2MPO_4F (A = Li, Na; M = Mn, Fe, Co, Ni) family provides one of the largest playgrounds for searching new cathode materials[5]. From the electrochemical standpoint, this class also regains interest due to a theoretical possibility of multi-electron redox transitions enabling reversible de/intercalation of more than one alkali ion per transition metal center.

The wide structural variety of A_2MPO_4F is primarily originated from multiple options in playing with the chemical composition of the cation sublattice. Depending on the nature of the A and M metals, MO_4F_2 octahedra (key building blocks) constitute various types of linkage: from corner-sharing to face-sharing and their combinations. Since A and M sites can be populated by more than one element type, altering their average ionic radius by substitutions might also influence the preferable MO_4F_2 connectivity thus preserving a specific structural type for new chemical compositions or even giving rise to new structures.

Corner-shared MO_4F_2 octahedra are only characteristic to Na_2MnPO_4F[6,7] and its limited solid-solution with Fe[8] where they are connected by fluorine atoms to form infinite 1D-chains bonded by PO_4 tetrahedra into a 3D framework. Edge-shared octahedra are intrinsic to a larger number of representatives: Li_2MPO_4F (M = Co, Ni)[9–13], $Li_{1.3}Na_{0.7}NiPO_4F$[14], and $LiNaMPO_4F$ (M = Fe, Co)[15–18] are isostructural and adopt a 3D framework with MO_4F_2 octahedra. $LiNaNiPO_4F$ adopts a quasi-layered structure, with MO_4F_2 octahedra being connected via O–F edges[14]. Na_2MPO_4F (M = Fe, Co, Ni) reveals a more complicated linkage of MO_4F_2 octahedra: the structures are built upon $M_2O_6F_3$ bioctahedral units comprising face-shared MO_4F_2 octahedra, which are bridged by corners to form zig-zag chains[5,14,19]. At the same time, a known

[a] Dr. Stanislav S. Fedotov, Dr. Dmitry A. Aksyonov, Prof. Keith J. Stevenson, Prof. Artem M. Abakumov
Skoltech Center for Energy Science and Technology, Skolkovo Institute of Science and Technology, 121205 Moscow, Russian Federation.
[b] Aleksandr Sh. Samarin, Dr. Nellie R. Khasanova, Prof. Evgeny V. Antipov
Department of Chemistry, Lomonosov Moscow State University, 119991 Moscow, Russian Federation.
[c] EMAT, University of Antwerp, Groenenborgerlaan 171, B-2020, Antwerp, Belgium
* Corresponding authors: s.fedotov@skoltech.ru; antipov@icr.chem.msu.ru

high-pressure form of Na_2CoPO_4F consists of edge-shared CoO_4F_2 octahedra[20].

Indeed, the MO_4F_2 octahedra ordering vastly influences the accommodation options for alkali ions, shaping their diffusion pathways and governing the electrochemical behavior of the material. Moreover, the arrangement of octahedra regulates the M–O,F bond lengths, which contributes to determining the electrochemical potential of the specific M^{3+}/M^{2+} redox transition.

In practice, fluoride-phosphate-based cathode materials with earth-abundant compositions (i.e. containing Fe and/or Mn) have unclear perspective because of either insufficient potential of the Fe^{3+}/Fe^{2+} redox pair [21–24], which does not compensate the loss of specific capacity due to a heavy PO_4F anionic moiety in comparison to oxides, or because of a Jahn-Teller distortion of Mn^{3+} typically leading to huge cell volume variations and consequently fast degradation of Mn-based materials[25–27]. Ni-based fluoride-phosphates exhibit enormously high redox potentials which are far beyond the stability range of electrolytes[13,28]. In turn, Co-containing fluoride-phosphates operate at the edge of the electrolyte stability window and hold promise to be implemented in next-generation batteries relying on the recent advances in high-voltage electrolytes[29–32].

In this work, we present a new layered form of $LiNaCoPO_4F$ fluoride-phosphate isostructural to $LiNaNiPO_4F$ with chains of edge-shared octahedra, which was stabilized by adjusting the temperature conditions. This finding shows that synthesis temperature remains an “unexplored dimension” for chemistry of the A_2MPO_4F fluoride-phosphates and requires careful examination.

Results and Discussion

Synthesis and thermal analysis

According to the literature, the A_2MPO_4F fluoride-phosphates can be synthesized via one- or two-step procedure, with the latter including preliminary preparation of an $AMPO_4$ intermediate. In the case of $LiNaCoPO_4F$ such a precursor was chosen to be $LiCoPO_4$, adopting the olivine structure, which is quite easily synthesized by a freeze-drying-assisted solid-state route. The X-ray powder diffraction (XRD) pattern of the resulting $LiCoPO_4$ sample is presented in Figure 1, A. The sample contains no traceable admixtures.

Taking into account the structural diversity in this family and its possible dependence not only on the nature of A alkali cations, but also on the temperature conditions of the synthesis, we first performed a DSC study of the $LiCoPO_4$+NaF mixture in the 30-650°C temperature range to find heat effects corresponding to phase formation. It should be noted that at temperatures over 650°C the sample starts melting.

A broad endothermic process can be observed in the DSC curve (Figure 1, B) with onset and offset temperatures of ~500°C and 630°C. In fact, it can be described as two overlapping processes at 563 and 592°C.

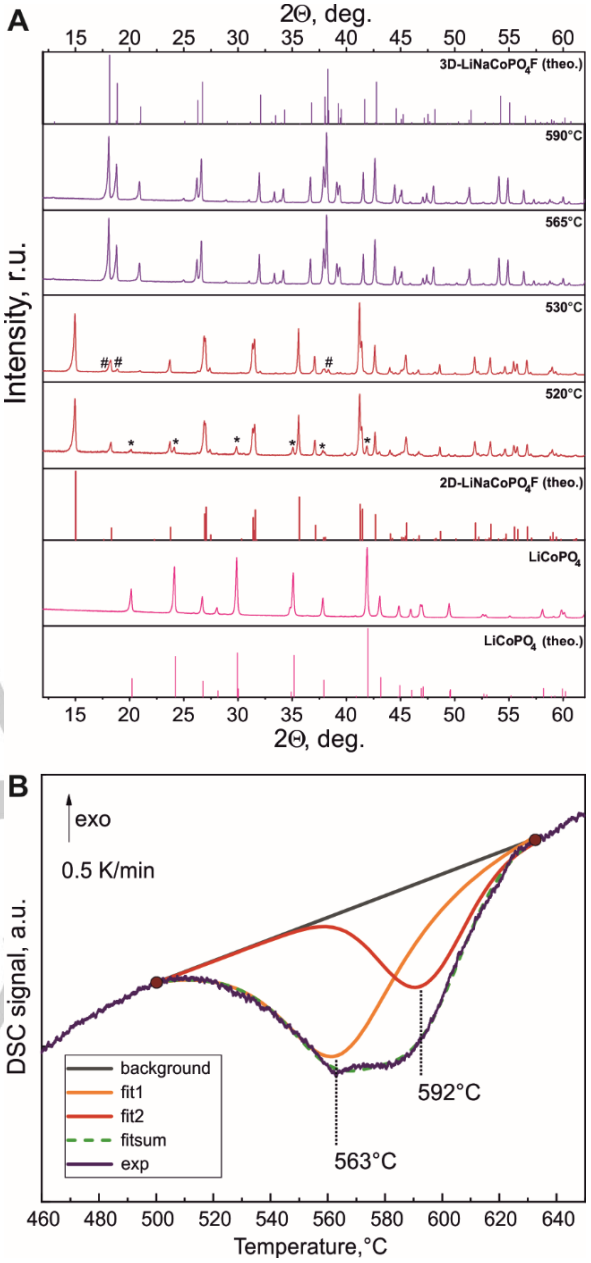

Figure 1. A) XRD patterns of the $LiCoPO_4$ and $LiCoPO_4$+NaF mixture annealed at 520, 530, 565, and 590°C for 3 hours. The asterisks “*” designate the reflections of the $LiCoPO_4$ admixture, # – reflections of 3D-$LiNaCoPO_4F$. B) DSC curve for the $LiCoPO_4$+NaF mixture in the 460-650°C temperature region (0.5 K/min heating rate) showing the endothermic process approximated with two peaks centred at 563 and 592°C.

In practice, annealing the mixture at 565°C or 590°C results in the known $LiNaCoPO_4F$ fluoride-phosphate with a three-dimensional polyhedral framework (ICSD 424194, S.G. #62 *Pnma*, a = 10.9274(1) Å, b = 6.30007(5) Å, c = 11.35666(9) Å, V = 781.832(14) Å^3, further denoted as 3D-$LiNaCoPO_4F$). Since two endothermic processes largely overlap and the onset temperature for the second process is located around 550°C, further annealing was conducted at 530°C to avoid triggering the

second process centered at 592°C, which presumably corresponds to formation of 3D-$LiNaCoPO_4F$. The XRD patterns of the samples calcined at the three above-mentioned temperatures are collected in Figure 1, A. At 530°C a completely different XRD pattern is obtained that is closely related to the pattern of $LiNaNiPO_4F$ crystallizing in a quasi-layered (2D) monoclinic structure (ICSD 423847, S.G. #14, $P2_1/c$).

At further lowering of the annealing temperature (even by 10°C, to 520°C) the $LiCoPO_4$+NaF mixture does not fully react and slight amount of the initial $LiCoPO_4$ resides as an impurity phase. At the same time, at 530°C the sample already contains a minor amount of 3D-$LiNaCoPO_4F$ indicating a very narrow temperature range for stabilization of the 2D-phase. At heating above 560°C, the as-prepared 2D-$LiNaCoPO_4F$ irreversibly transforms into the 3D-$LiNaCoPO_4F$ modification. During cooling, no heat effect is observed on the DSC curve.

Crystal structure

The crystal structure of the 2D-$LiNaCoPO_4F$ (deposited in CCDC #1945013) obtained at 530°C was Rietveld-refined based on XRD data. The space group choice for the new $LiNaCoPO_4F$ fluoride-phosphate (further denoted as 2D-$LiNaCoPO_4F$) was validated by electron diffraction: selected area electron diffraction (SAED) patterns along the main zone axes clearly demonstrate *h*0*l*: *l* = 2n, and 0*k*0: *k* = 2n reflection conditions (Figure 2), in agreement with the space group $P2_1/c$.

The X-ray diffraction pattern was fully indexed on a monoclinic lattice (S.G. #14 $P2_1/c$) with a = 6.83881(4) Å, b = 11.23323(5) Å, c = 5.07654(2) Å, β = 90.3517(5) °, V = 389.982(3) Å^3 (Figure 3). The 3D-$LiNaCoPO_4F$ impurity was included in the refinement (1.8% wt.).

Table 1. Crystallographic data and parameters of the Rietveld refinement for 2D-$LiNaCoPO_4F$.

Formula	$LiNaCoPO_4F$
Space group	$P2_1/c$
a, Å	6.83881(4)
b, Å	11.23323(5)
c, Å	5.07654(2)
β,°	90.3517(5)
V, Å^3	389.982(3)
Z	4
Radiation	X-rays, Co-$K_{\alpha1}$, λ = 1.78896 Å
2θ range, step, deg.	10-100, 0.01
GOF	1.28
R_I, %	2.20
Rp, Rwp, %	2.22, 3.25

Table 2. Atomic positions, fractional coordinates and isotropic displacement parameters for $LiNaCoPO_4F$.

Atom	*x/a*	*y/b*	*z/c*	U_{iso}, Å^2	BVS
Na	0.5130(2)	0.16606(7)	0.7561(4)	0.0257(3)	0.995(2)
Li	-0.2692(7)	0.0806(4)	0.2561(12)	0.0059(12)	1.018(7)
Co	-0.01705(9)	0.16907(3)	0.7346(2)	0.01551(13)	1.980(3)
P	0.24345(12)	0.08015(7)	0.2269(2)	0.0078(2)	4.891(10)
O1	0.45386(15)	0.12456(7)	0.2571(4)	0.01907(10)	1.962(6)
O2	0.1034(2)	0.17195(13)	0.3523(3)	0.01907(10)	1.933(6)
O3	0.1982(2)	0.06904(13)	-0.0729(3)	0.01907(10)	1.893(7)
O4	0.2204(2)	-0.04175(13)	0.3611(3)	0.01907(10)	2.055(7)
F	-0.2115(2)	0.28703(9)	0.5346(3)	0.0249(4)	1.041(4)

Main crystallographic parameters, atomic positions, atomic displacement parameters and selected interatomic distances are presented in Tables 1-3. The [001] HAADF-STEM image (Figure 2) confirms the refined structure. In this image, brightest dots correspond to the projections of the Co columns, weaker ones to P columns. The Na and O columns are virtually invisible because of their low atomic numbers.

Table 3. Selected interatomic distances for $LiNaCoPO_4F$.

Bond	Distance, Å	Bond	Distance, Å
Na–O1	2.602(3)	Co–O2	2.0485(15)
Na–O1	2.623(3)	Co–O2	2.1004(16)
Na–O1	2.3870(11)	Co–O3	2.0890(16)
Na–O3	2.571(2)	Co–O4	2.0499(16)
Na–O4	2.375(2)	Co–F	2.1312(13)
Na–F	2.5845(18)	Co–F	2.0897(15)
Na–F	2.406(2)	P–O1	1.5291(12)
Li–O1	1.963(5)	P–O2	1.5629(16)
Li–O3	1.989(5)	P–O3	1.5543(17)
Li–O4	2.024(6)	P–O4	1.5365(16)
Li–F	1.892(5)		
Li–O2	2.774(5)		
Li–F	2.736(5)		

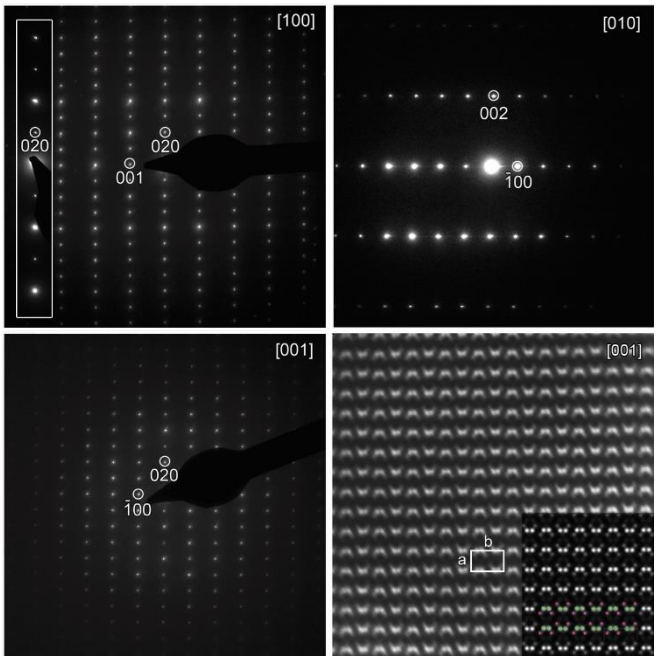

Figure 2. SAED patterns along [100], [010] and [001] main zone axes. The presence of reflections 0*k*0: *k* = 2*n*+1 or 00*l*: *l* = 2*n*+1 in [100] and [001] is caused by double diffraction, as demonstrated by the absence of those *00l* reflections on the [010] pattern and the absence of those *0k0* reflections in the inset at the left side of the [100] pattern obtained by tilting around the b* axis from a (different) [100] pattern. A low bandpass filter was applied to the experimental image. The calculated image is added in the lower right corner, with Co and P atoms indicated in green and pink, respectively. The white rectangle marks the unit cell.

The 2D-$LiNaCoPO_4F$ polymorph is isostructural to $LiNaNiPO_4F$. It crystallizes with a quasi-layered (2D) structure, consisting of $CoPO_4F$ slabs with the lithium and sodium atoms accommodated in the interlayer space in the ordered manner. The CoO_4F_2 octahedra are slightly distorted and linked by the O2–F edge to form zig-zag chains along the *c* axis. These chains are connected by the PO_4 tetrahedra, which are quite regular, with P–O distances ranging from 1.5291(12) Å to 1.5629(16) Å. The average P–O interatomic distance is equal to 1.546 Å. Co^{2+} is highly likely in a high-spin (HS) state, which is expected from the low-field ligand environment and agrees with the average interatomic distances being characteristic to the HS configuration, and further confirmed using DFT+U calculations. The HS state of the M^{2+} cation in analogous A_2MPO_4F fluoride-phosphates was also confirmed by magnetic susceptibility measurements[16,17].

Li occupies an octahedral void and is shifted from its geometrical center towards the so-called "dangling" O1 atom (belonging to the PO_4 tetrahedra only and not constituting the metal octahedra) of the PO_4 tetrahedra. The resulting coordination for Li should be preferentially regarded as tetrahedral (Figure 4, B) whereas it comprises only four normal Li–O/F bonds (Table 3). The BVS for Li was calculated considering additional long bonds at ~2.7 Å (Table 3) to be 1.018(7), which is close to 1 showing no under/over-bonding contrary to many Li-containing A_2MPO_4F. For instance, one of three Li positions in Li_2CoPO_4F is very under-bonded, while two others are over-bonded[33]. The coordination of the Na site can be considered as a distorted pentagonal bipyramid with two F atoms in *cis* configuration, or a single-cap octahedron (Figure 4, B). In comparison to Li, the Na position is surrounded by three "dangling" O1 oxygen atoms from the PO_4 groups. The BVS values for all sites are in good agreement with the expected oxidation states (Table 2).

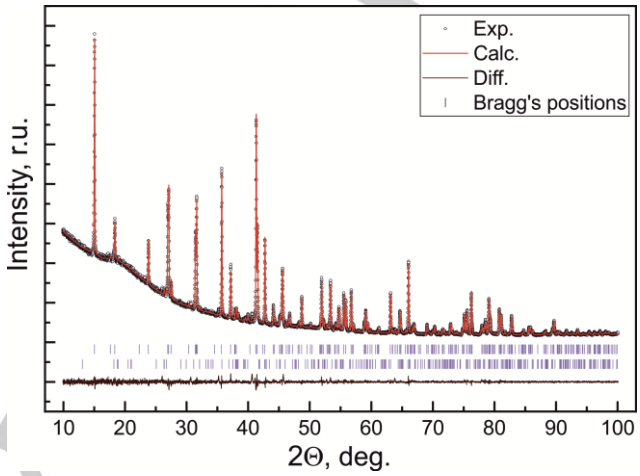

Figure 3. Experimental, calculated and difference XRD patterns after the Rietveld refinement of 2D-$LiNaCoPO_4F$. Bragg reflections are denoted as light-green bars for 2D (top) and 3D- $LiNaCoPO_4F$ as an impurity of 1.8% mass (bottom).

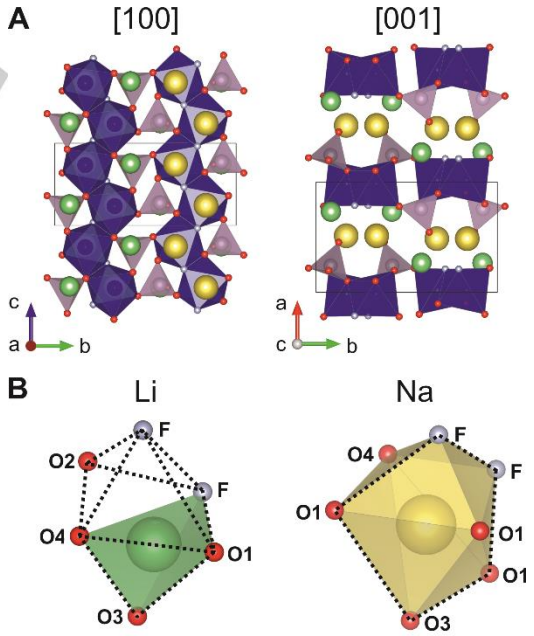

Figure 4. A) [100] and [001] projections of the 2D-$LiNaCoPO_4F$ crystal structure. CoO_4F_2 octahedra are blue, PO_4 tetrahedra are grey, oxygen atoms are shown in red, fluorine atoms - in grey, Na atoms - in yellow, Li - in green. B) A graphical representation of the alkali atom site coordination in 2D-$LiNaCoPO_4F$. Dotted lines show the octahedral void for Li and the 5-coordinated basal plane of the NaO_5F_2 bipyramid.

According to SEM data, 2D-LiNaCoPO$_4$F consists of ill-shaped particles of 200-700 nm (Figure 5). Such a broad particle size distribution may originate from partial coalescence of the particles during the synthesis at high temperatures due to NaF, which promotes surface melting acting as a flux. Nevertheless, the chemical composition of the particles correspond to the ascribed formula of 2D-LiNaCoPO$_4$F: SEM-EDX shows Na:Co:P ratio collected from 3 areas to be 0.95(8):1.00(5):1.11(9). STEM-EDX mapping reveals that Na, Co, P, O, F are homogeneously distributed over the particles (Figure 6).

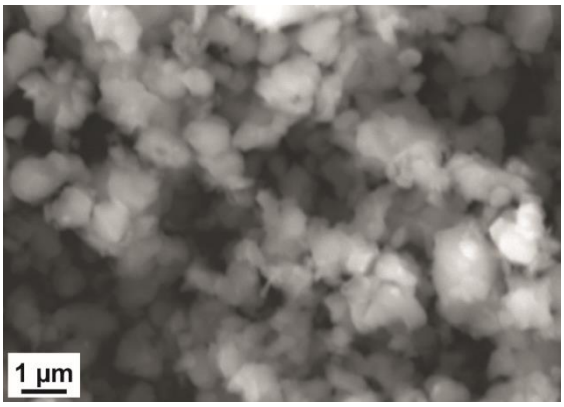

Figure 5. SEM micrograph of 2D-LiNaCoPO$_4$F.

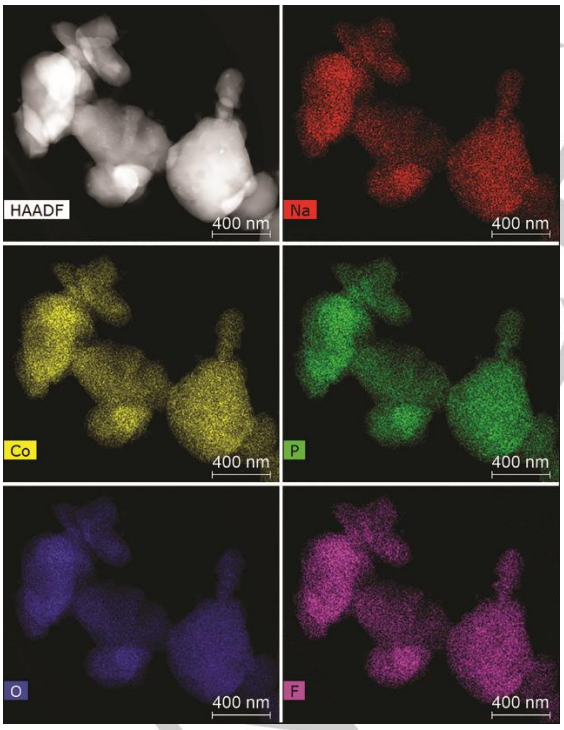

Figure 6. HAADF-STEM micrograph and STEM-EDX maps of Na, Co, P, O, and F for 2D-LiNaCoPO$_4$F.

DFT calculations

To reveal the influence of the structural type on volume changes, redox potentials, cation migration, and spin state of Co we performed DFT+U/DFT calculations using experimental crystal structures as a starting point.

Lattice parameters

The lattice constants calculated with DFT and DFT+U methods, for 2D- and 3D-LiNaCoPO$_4$F in different deintercalated states and different spin states of Co, as well as the experimental values are collected in Table 4. DFT without U and DFT+U give minor differences in calculated cell parameters. However, the difference between high spin (HS) and low spin (LS) Co states is more pronounced, with lattice constants for LS on average 1% lower than those for HS.

Table 4. Lattice constants (Å) and volume (Å^3) for 2D and 3D phases, calculated with DFT without U and DFT+U methods. CP stands for CoPO$_4$F.

	State	Method	*a*, Å	*b*, Å	*c*, Å	*β*, Å	*V*, Å^3
2D	LiNaCP	Exp.	6.839	11.233	5.077	90.352	389.98
		PBE	6.88	11.31	5.1	90.55	396.8
		PBE+U (HS)	6.88	11.33	5.12	90.47	398.9
		PBE+U (LS)	6.83	11.22	5.11	90.19	391.4
	Li□CP	PBE+U (HS)	7.16	11.11	5.04	89.72	400.3
		PBE+U (LS)	7	10.85	4.92	89.74	373.6
	□NaCP	PBE+U (HS)	7.14	11.24	5.02	90.78	402.6
		PBE+U (LS)	7.07	10.89	4.88	89.8	375.9
3D	LiNaCP	Exp.	10.911	6.278	11.333	90	776.3
		PBE	10.97	6.35	11.41	90	794.5
		PBE+U (HS)	10.98	6.33	11.41	90	794
	Li□CP	PBE+U (HS)	10.84	6.29	11.14	90	759.1
	□NaCP	PBE+U (HS)	11.04	6.4	11.17	90	790.2

Generally, the PBE flavor of the exchange-correlation potential overestimates experimental lattice constants of phosphates by 1-2% [34–36]. Considering a similar behavior of PBE for the LiNaCoPO$_4$F phases, the cell parameters for Co^{2+} in a high spin state indeed exceed the experimental values by 0-2%, confirming that Co^{2+} is in a high spin state, which was also previously

validated by magnetic susceptibility measurements for 3D-$LiNaCoPO_4F$[17].

Concluding from the total energies, the 2D lattice with HS Co^{2+} is by 0.1 eV/atom more stable than that with LS Co^{2+}. The same picture is observed for the deintercalated phases, whose HS states are more stable only by 0.05 eV/atom though.

Interestingly, in the case of the 2D phase after extraction of either Li or Na the volume only slightly increases by 0.9 or 0.4 %, respectively. The volume change is surprisingly small for Na, given that for phosphates this value is typically around 4-6%. In the case of the 3D phase, the volume variation is much larger, >4%. Low variation of the cell volume upon deintercalation is highly important for stable cycling of cathode material preventing its degradation due to stress-induced cracking.

Stability of phases and intercalation potentials

Comparison of total energies for 2D and 3D phases shows that in the initial ("discharged") state the 3D phase is slightly more stable (by 0.007 eV/atom), however after extraction of all Na the 2D phase becomes notably more stable (by 0.02 eV/atom).

The average intercalation potentials in 2D for LiNaCP/Li□CP and LiNaCP/□NaCP are 4.1 V and 4.4 V, respectively. The smaller average potential for Na deintercalation implies that it should be extracted in the first place. This agrees with our previous work on closely-related Na_2FePO_4F (*Pbcn*), where it was shown that during charging in a Li-ion cell, Na is extracted and substituted with Li[36]. Therefore, regardless of whether Fe or Co is used as a redox center, the average potential for Na is lower by ~0.3 V than that of Li.

The average intercalation potential in 3D for LiNaCP/Li□CP is 4.3 V, higher by 0.2 V compared to the 2D phase, which is in agreement with the experimental results. The extraction of Li occurs at 4.5 V.

Migration barriers

The migration barriers for Li and Na vacancies are calculated using DFT without U method. It was shown in our previous paper, that employment of Hubbard U correction has only minor influence on migration barriers, yet significantly worsens convergence of wave function[34].

The considered migration hops in the 2D and 3D phases are shown in Figure 7, the migration barriers are collected in Tables 5-7. In the 2D phase, the one-dimensional diffusion of vacancies can easily occur along the *c* axis for both Li and Na. The diffusion of Na in the 3D phase is hindered; the minimum migration barrier is increased up to 0.45-0.5 eV, which manifests the diffusion coefficients to be several orders of magnitude lower than those in 2D. At the same moment, the diffusion of Li is possible in the 3D phase as well, with the migration barrier of 0.2 eV and substitution of Na on diffusion.

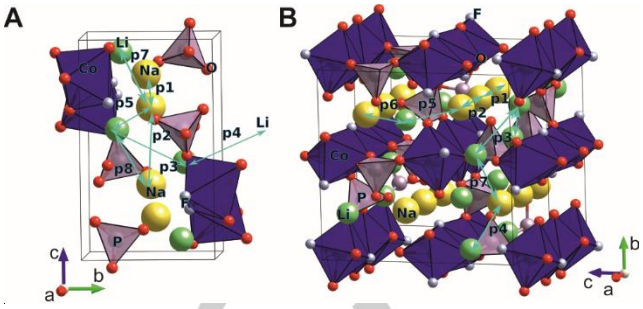

Figure 7. Considered migration hops in A) 2D phase and B) 3D phase.

Table 5. The hopping distance in initial lattice, d (Å), and corresponding migration barriers of Li and Na vacancy in the 2D phase. Migration barriers for p6 (3.18 Å) and p8 (4.84 Å) hops are more than 0.8 eV and not shown. For p5 and p7 the arrow shows the direction of ion migration.

Hop	d, Å	Barrier, eV	
		Na	Li
p1 Na–Na	3.19	0.15	0.15
p2 Na–Na	4.56	1.5	0.9
p3 Li–Li	4.49	-	1.2
p4 Li–Li	4.72	-	1.2
p5 Na→Li/Li→Na	3.07	0.5	0.4
p7 Na→Li/Li→Na	3.22	1.0	0.55
p8 Li→Na	3.32	0.3	0.85

Table 6. The hopping distance in the initial lattice (d, Å), and corresponding migration barriers of Li and Na vacancy in the 3D phase. Li–Li hops are not relevant. For p4-p7 the arrow shows the direction of ion migration, the vacancy migration direction is opposite.

Hop	d, Å	Barrier	
		Na	Li
p1 Na–Na	3.06	0.4	0.05
p2 Na–Na	3.28	0.5	0.2
p4 Na→Li/Li→Na	3.2	0.4	0.25
p5 Na→Li/Li→Na	3.24	0.75	0.6
p6 Na→Li/Li→Na	3.34	0.25	0.3
p7 Na→Li/Li→Na	3.5	0.45	0.8

Table 7. Pathways for continuous transport of Na/Li along main crystallographic axes and their effective migration barriers (eV) for 2D and 3D phases.

Diffusion direction	Hops		ΔE_{eff}, eV	
	2D	3D	2D	3D
[100]	p3-p4 (Li)	p4-p7 (Na)	1.2	**0.45 (Na)**
[010]	p1-p2 (Na) p5-p8-p1 (Na, Li)	p1-p2 (Na) p1-p2 (Li)	1.5 0.85/0.4	0.5 **0.2 (Li)**
[001]	p1-p1 (Na) p1-p1 (Li)	p5-p6 (Na)	**0.15 (Na)** **0.15 (Li)**	0.7

Stability of phases on temperature

The synthesis of the phases is performed at relatively high temperatures: 530-540 °C for 2D and 600 °C for 3D. To estimate the influence of temperature on free energy, the phonon band structure was calculated and free energy is then extracted. The dependence of free energy on temperature for 2D and 3D phases is shown in Figure 8. It is seen that with the increase of temperature the free energy of both phases decreases due to vibrational entropy. However, if at 0K the 3D phase is slightly more stable than 2D, at 712 K the 2D phase stabilizes and at 1000K becomes by 0.003 eV/atom more stable. Therefore, the vibrational entropy arguments could not be used to explain the reasons of the 3D phase stabilization during synthesis at higher temperatures.

Electrochemical measurements

Attempts to carbon-coat 2D-$LiNaCoPO_4F$ failed due to either its conversion to 3D-$LiNaCoPO_4F$ or decomposition yielding a significant amount of metallic Co. Consequently, all preliminary electrochemical measurements were carried out with a pure uncoated 2D-$LiNaCoPO_4F$ sample.

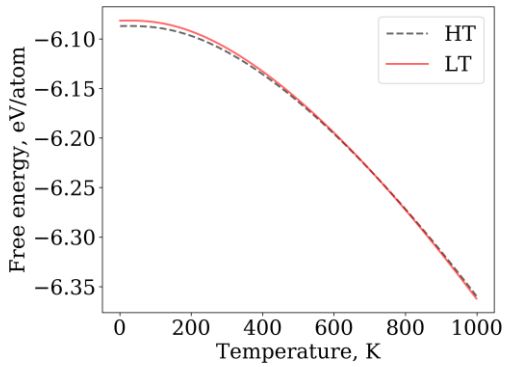

Figure 8. Dependence of free energy on temperature calculated with density functional perturbation theory for the 2D (LT) and 3D (HT) phases.

Galvanostatic measurements of 2D-$LiNaCoPO_4F$ revealed reversible electrochemical activity in both Li and Na cells (Figure 9) with a huge portion of irreversible capacity presumably related to electrolyte decomposition at high potentials.

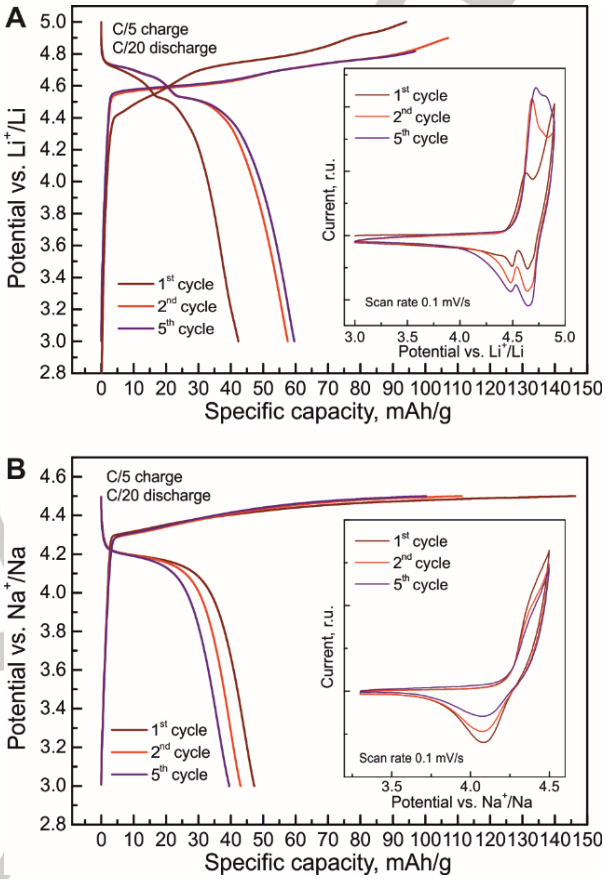

Figure 9. Galvanostatic charge-discharge curves for pure 2D-$LiNaCoPO_4F$ in A) Li-ion cell (first charge to 5.0 V, second to 4.9 V, third and subsequent – to 4.8 V vs. Li^+/Li) and B) Na-ion cell in the 3.0-4.5 V vs. Na^+/Na potential range. Insets: CV curves for 2D-$LiNaCoPO_4F$ in Li cell (top) and Na cell (bottom).

The average potential of 2D-$LiNaCoPO_4F$ in a Li-ion cell is located around 4.5 V, the material delivers the specific capacity of 62 mAh/g, whose growth on cycling might be presumably caused by gradual electrochemical Li substitution for Na altering the shape of the curves as it was shown for analogous Na-containing fluoride-phosphate systems[15,21]. In Na-ion cell, the profile of charge-discharge curves does not depend on cycle number, possibly indicating that within the 3.0-4.5 vs. Na^+/Na potential range Li ions in 2D-$LiNaCoPO_4F$ do not participate in electrochemical de/intercalation. The specific capacity amounts to 48 mAh/g at the first cycle and quickly fades on cycling. The average potential in a Na-ion cell is equal to ~4.2 V in accordance with the theoretical value calculated by DFT+U. This is 0.2 V less than that of Na_2CoPO_4F[19] with corner/face-shared octahedra emphasizing the influence of MO_4F_2 octahedra connectivity on the Co^{3+}/Co^{2+} redox potential.

Conclusions

A novel fluoride-phosphate, $LiNaCoPO_4F$ with a layered (2D) crystal structure was synthesized using a freeze-drying-assisted solid-state technique. It can be stabilized in quite a narrow temperature range around 520°C as confirmed by the DSC analysis. Above 530°C, an irreversible transformation of 2D-$LiNaCoPO_4F$ into a 3D-framework modification is observed. As shown by DFT+U calculations both 2D and 3D phases are very close in energy. The refinement of the crystal structure revealed that 2D-$LiNaCoPO_4F$ is isostructural to $LiNaNiPO_4F$ with edge-shared MO_4F_2 octahedra. Topologically, 2D-$LiNaCoPO_4F$ is closely related to the Na_2CoPO_4F representative with corner-shared bioctahedra being the product of Li replacement by larger Na, which pushes apart the MO_4F_2 octahedra inducing their collapse to form $M_2O_6F_3$ bioctahedra units instead of edge-shared $(MO_4F_2)_\infty$ chains. The reported results also imply that the $LiNaNiPO_4F$ structural type can adopt other chemical compositions and/or solid solutions provided that the required average radius of cations in the M site is maintained as well as appropriate temperature conditions are chosen. The 2D-$LiNaCoPO_4F$ framework also gives promise as a basis for designing new positive electrode materials with expected fast ion transport as shown by DFT calculations revealing extremely low energy barriers for Li and Na ion migration (~0.15 eV), lower than that in the 3D phase. Another important fact is that after Na deintercalation the calculated volume variation is extremely small for 2D-$LiNaCoPO_4F$ not exceeding 1% that anticipates stable cycling without severe mechanical degradation.

In case of 2D-$LiNaCoPO_4F$ the primary problem to be solved is creating a carbon coating preserving the structure in order to realize better electrochemical performance. The currently achieved relatively modest specific capacity of the 2D-$LiNaCoPO_4F$ cathode material can be increased by carbon coating, which usually significantly improves electrochemical performance. The full potential of Na-ion fluoride-phosphates as cathode materials is to be revealed in the future whereas this study demonstrates that fine-tuning of synthesis conditions allows to stabilize specific structural types for other chemical compositions and to possibly find novel structures with unique characteristics for rechargeable batteries.

Experimental Section

Synthesis

The $LiNaCoPO_4F$ samples with 2D and 3D structures were synthesized via a two-step freeze-drying assisted solid-state method. At first, $LiCoPO_4$ was prepared as described in [9] and then mixed with 3% excess of NaF (99.9%, Sigma-Aldrich), pressed into pellets and annealed under Ar flow at different temperatures from 500 to 650°C depending on the structure for 1 h with subsequent quenching to room temperature (under Ar atmosphere).

Material characterization

X-ray powder diffraction patterns were collected with a STOE STADI-P powder diffractometer (Co-$K_{\alpha1}$ radiation, 10-100° 2θ range) and a Guinier Camera Huber G670 (Co-$K_{\alpha1}$ radiation, 5-100° 2θ range).

The energy-dispersive X-ray analysis (EDX) was performed on a scanning electron microscope (SEM) JEOL JSM-6490LV (W-cathode, operating at 30 kV) equipped with an energy dispersive X-ray (EDX) system INCA Energy+ (Oxford, Si-(Li)-detector).

Differential scanning calorimetry (DSC) analysis was carried out with a TG-DSC STA-449 apparatus (Netzsch, Germany) under Ar (50 ml/min) or dry air (50ml/min) flow. The powders were treated at 0.5-2 K/min heating rates in the 35-650°C temperature ranges.

For the transmission electron microscopy (TEM) studies, a small amount of the samples was grinded using an agate mortar under ethanol. The resulting suspension was deposited onto a copper grid covered with a holey carbon layer. The TEM study was performed at FEI Tecnai G2 and FEI Tecnai Osiris microscopes operated at 200kV equipped with a Super-X detector. High resolution STEM images were acquired at a FEI Titan^3 microscope operated at 300 kV. The simulation of STEM images was performed using QSTEM software.

Structure analysis and cell parameters refinement

The Rietveld refinement of the 2D-$LiNaCoPO_4F$ structure based on powder X-ray diffraction data was performed in JANA2006[37] program package with the $LiNaNiPO_4F$ structure (S.G. $P2_1/c$, #14) as an initial model[14]. The background was estimated by a set of Legendre polynomials, followed by fitting of the cell parameters and the peaks' shape with Pseudo-Voigt function. After full profile matching, scale factors, atomic coordinates and isotropic atomic displacement parameters (ADPs) were refined. Refinement of the Na site occupancy resulted in a negligible deviation from 1, so it was further fixed to 1. For the final refinement, all ADPs were constrained to be equal for the sites occupied by the same type of element. The crystal structures were drawn using the VESTA visualization system[38]. Cell parameters for the 3D-$LiNaCoPO_4F$ were refined in JANA2006 using Le Bail method.

Electrochemical measurements

For electrochemical testing, electrodes were prepared by mixing 65 wt. % of $LiNaCoPO_4F$ active material, 22 wt. % acetylene black (carbon Super-C) and 13 wt. % polyvinylidene fluoride (PVDF). N-Methyl pyrrolidinone (NMP) was added to dissolve PVDF. The resulting slurry was cast on the aluminum foil by the Dr. Blade® technique. The electrodes were dried in vacuum at 80°C for 3h to remove H_2O and NMP. Average mass loading of the active material was 3-4 mg/cm^2. The electrochemical properties of $LiNaCoPO_4F$ were evaluated in Li and Na-ion cells using Swagelok-type two-electrode cells with a commercial 1M $LiPF_6$ (Sigma-Aldrich) or 1M $NaClO_4$ in EC:DEC (1:1 by vol.) electrolytes, glass fiber separators and Li or Na metal (Sigma-Aldrich) used as anodes. The charge/discharge and cyclic voltammetry measurements were made at room temperature using a Biologic VMP3 potentiostat.

DFT calculations

All DFT calculations were performed in the VASP program [39] using the generalized gradient approximation (GGA) to exchange-correlation functional and standard PAW PBE potentials[40] with minimum number of valence electrons. To take into account the strongly correlated character of the d-electrons of Co, a Hubbard-like correction is added within the Dudarev scheme and U value of 3.4 eV. Gaussian smearing with a

smearing width of 0.1 eV was used for Brillouin-zone integrations. The energy cut-off was fixed at 400 eV. To eliminate Pulay errors the lattice optimization (ISIF = 4) was performed at constant volume for several contracted and expanded cells (7 points).

The migration barriers were determined using nudged elastic band (NEB) method as implemented in VASP. For 2D and 3D phases, the 144-atom 2×1×2 and 1×2×1 supercells with gamma-centered k-point 2×2×3 and 2×2×2 meshes were used, respectively. The NEB method allows finding minimum energy path, which includes several intermediate configurations (images) between initial and final states. Five intermediate images were used. The optimization of atomic positions was performed using quasi-Newton algorithm until the maximum force permitted for any vector component was less than 0.1 eV/Å. The computational setup, including errors due to the periodic boundary conditions has been estimated to provide the precision of 0.1 eV for migration barriers.

To account for the contribution of lattice vibrations to the free energies, the harmonic approximation was employed, as implemented in the PHONOPY code[41]. The force constants were calculated using density functional perturbation theory with increased FFT meshes in VASP for 144-atom supercells.

Acknowledgments

This work is supported by Russian Science Foundation (grant 17-73-30006). The authors greatly thank Dr. D. Rupasov for TG-DSC experiments, B. D. Shmykov and A. I. Manoilov for assistance with samples preparation, Skoltech Center for Energy Science and Technology and Moscow State University Program of Development up to 2020. J. Hadermann and O. M. Karakulina acknowledge support from FWO under grant G040116N

Keywords: Fluoride-phosphates, rechargeable batteries, electrode materials, high voltage cathodes

[1] K. Mizushima, P. C. Jones, P. J. Wiseman, J. B. Goodenough, *Mater. Res. Bull.* **1980**, *15*, 783–789.

[2] A. K. Padhi, K. S. Nanjundaswamy, J. B. Goodenough, *J. Electrochem. Soc.* **1997**, *144*, 1188.

[3] C. Masquelier, L. Croguennec, *Chem. Rev.* **2013**, *113*, 6552–6591.

[4] E. V. Antipov, N. R. Khasanova, S. S. Fedotov, *IUCrJ* **2015**, *2*, 85–94.

[5] B. L. Ellis, W. R. M. Makahnouk, W. N. Rowan-Weetaluktuk, D. H. Ryan, L. F. Nazar, *Chem. Mater.* **2010**, *22*, 1059–1070.

[6] O. V. Yakubovich, O. V. Karimova, O. K. Mel'nikov, IUCr, *Acta Crystallogr. Sect. C Cryst. Struct. Commun.* **1997**, *53*, 395–397.

[7] S. W. Kim, D. H. Seo, H. Kim, K. Y. Park, K. Kang, *Phys. Chem. Chem. Phys.* **2012**, *14*, 3299–3303.

[8] N. Recham, J.-N. Chotard, L. Dupont, K. Djellab, M. Armand, J.-M. Tarascon, *J. Electrochem. Soc.* **2009**, *156*, A993.

[9] S. S. Fedotov, A. A. Kabanov, N. A. Kabanova, V. A. Blatov, A. Zhugayevych, A. M. Abakumov, N. R. Khasanova, E. V. Antipov, *J. Phys. Chem. C* **2017**, *121*, 3194–3202.

[10] S. Okada, M. Ueno, Y. Uebou, J. I. Yamaki, *J. Power Sources* **2005**, *146*, 565–569.

[11] M. Dutreilh, C. Chevalier, M. El-Ghozzi, D. Avignant, J. M. Montel, *J. Solid State Chem.* **1999**, *142*, 1–5.

[12] N. R. Khasanova, O. A. Drozhzhin, S. S. Fedotov, D. A. Storozhilova, R. V. Panin, E. V. Antipov, *Beilstein J. Nanotechnol.* **2013**, *4*, 860–867.

[13] S. Lee, S. S. Park, *J. Solid State Chem.* **2013**, *204*, 329–334.

[14] H. Ben Yahia, M. Shikano, S. Koike, K. Tatsumi, H. Kobayashi, *Dalt. Trans.* **2012**, *41*, 5838–5847.

[15] N. R. Khasanova, O. A. Drozhzhin, D. A. Storozhilova, C. Delmas, E. V Antipov, *Chem. Mater.* **2012**, *24*, 4271–4273.

[16] H. Ben Yahia, M. Shikano, S. Koike, K. Tatsumi, H. Kobayashi, H. Kawaji, M. Avdeev, W. Miiller, C. D. Ling, J. Liu, et al., *Inorg. Chem.* **2012**, *51*, 8729–8738.

[17] H. Ben Yahia, M. Shikano, H. Sakaebe, S. Koike, M. Tabuchi, H. Kobayashi, H. Kawaji, M. Avdeev, W. Miiller, C. D. Ling, *Dalt. Trans.* **2012**, *41*, 11692–11699.

[18] F. C. Strobridge, R. J. Clément, M. Leskes, D. S. Middlemiss, O. J. Borkiewicz, K. M. Wiaderek, K. W. Chapman, P. J. Chupas, C. P. Grey, *Chem. Mater.* **2014**, *26*, 6193–6205.

[19] K. Kubota, K. Yokoh, N. Yabuuchi, S. Komaba, *Electrochemistry* **2014**, *82*, 909–911.

[20] F. Sanz, C. Parada, C. Ruíz-Valero, *J. Mater. Chem.* **2001**, *11*, 208–211.

[21] B. L. Ellis, W. R. M. Makahnouk, Y. Makimura, K. Toghill, L. F. Nazar, *Nat. Mater.* **2007**, *6*, 749–753.

[22] Y. Kawabe, N. Yabuuchi, M. Kajiyama, N. Fukuhara, T. Inamasu, R. Okuyama, I. Nakai, S. Komaba, *Electrochem. commun.* **2011**, *13*, 1225–1228.

[23] J. Zhou, J. Zhou, Y. Tang, Y. Bi, C. Wang, D. Wang, S. Shi, *Ceram. Int.* **2013**, *39*, 5379–5385.

[24] M. Ramzan, S. Lebgue, P. Larsson, R. Ahuja, *J. Appl. Phys.* **2009**, *106*, 043510.

[25] Y. Zheng, P. Zhang, S. Q. Wu, Y. H. Wen, Z. Z. Zhu, Y. Yang, *J. Electrochem. Soc.* **2013**, *160*, A927–A932.

[26] X. Wu, J. Zheng, Z. Gong, Y. Yang, *J. Mater. Chem.* **2011**, *21*, 18630.

[27] X. Lin, X. Hou, X. Wu, S. Wang, M. Gao, Y. Yang, *RSC Adv.* **2014**, *4*, 40985–40993.

[28] M. Nagahama, N. Hasegawa, S. Okada, *J. Electrochem. Soc.* **2010**, *157*, A748.

[29] J. Wang, Y. Yamada, K. Sodeyama, C. H. Chiang, Y. Tateyama, A. Yamada, *Nat. Commun.* **2016**, *7*, 12032.

[30] X. Fan, L. Chen, X. Ji, T. Deng, S. Hou, J. Chen, J. Zheng, F. Wang, J. Jiang, K. Xu, et al., *Chem* **2018**, *4*, 174–185.

[31] J. Chai, J. Zhang, P. Hu, J. Ma, H. Du, L. Yue, J. Zhao, H. Wen, Z. Liu, G. Cui, et al., *J. Mater. Chem. A* **2016**, *4*, 5191–5197.

[32] H. Duncan, N. Salem, Y. Abu-Lebdeh, *J. Electrochem. Soc.* **2013**, *160*, A838–A848.

[33] N. R. Khasanova, A. N. Gavrilov, E. V. Antipov, K. G. Bramnik, H. Hibst, *J. Power Sources* **2011**, *196*, 355–360.

[34] D. A. Aksyonov, S. S. Fedotov, K. J. Stevenson, A. Zhugayevych, *Comput. Mater. Sci.* **2018**, *154*, 449–458.

[35] S. S. Fedotov, A. S. Samarin, V. A. Nikitina, D. A. Aksyonov, S. A. Sokolov, A. Zhugayevych, K. J. Stevenson, N. R. Khasanova, A. M.

Abakumov, E. V. Antipov, *J. Mater. Chem. A* **2018**, *6*, 14420–14430.

[36] I. V. Tereshchenko, D. A. Aksyonov, O. A. Drozhzhin, I. A. Presniakov, A. V. Sobolev, A. Zhugayevych, D. Striukov, K. J. Stevenson, E. Antipov, A. M. Abakumov, *J. Am. Chem. Soc.* **2018**, *140*, 3994–4003.

[37] V. Petříček, M. Dušek, L. Palatinus, *Zeitschrift für Krist. - Cryst. Mater.* **2014**, *229*, 345–352.

[38] K. Momma, F. Izumi, *J. Appl. Crystallogr.* **2011**, *44*, 1272–1276.

[39] G. Kresse, J. Furthmüller, *Comput. Mater. Sci.* **1996**, *6*, 15–50.

[40] J. P. Perdew, K. Burke, M. Ernzerhof, *Phys. Rev. Lett.* **1996**, *77*, 3865–3868.

[41] A. Togo, I. Tanaka, *Scr. Mater.* **2015**, *108*, 1–5.

10.1002/ejic.201900660

WILEY-VCH

Table of Contents

FULL PAPER

A novel layered polymorph of $LiNaCoPO_4F$ was stabilized by adjusting the synthesis temperature conditions. It gives promise for designing new positive electrode materials with fast ion transport and low volume variation for both Li- and Na-ion batteries. Synthesis temperature remains an “unexplored dimension” for the A_2MPO_4F fluoride-phosphates.

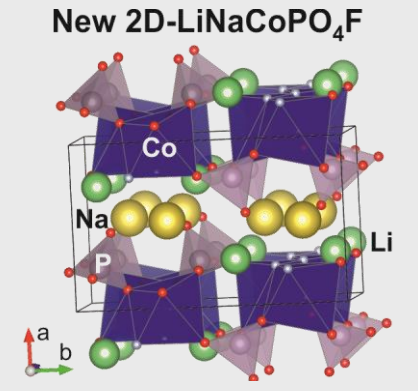

Rechargeable batteries

Stanislav S. Fedotov, Dmitry A. Aksyonov, Aleksandr Sh. Samarin, Olesia M. Karakulina, Joke Hadermann, Keith J. Stevenson, Nellie R. Khasanova, Artem M. Abakumov, Evgeny V. Antipov**

Tuning the crystal structure of A_2CoPO_4F (A = Li, Na) fluoride-phosphates: a new layered polymorph of $LiNaCoPO_4F$